Geometric and electronic structure of the Cs-doped Bi_2Se_3(0001) surface

M. M. Otrokov,[1,2,3,4] A. Ernst,[5,6] K. Mohseni,[5] H. Fulara,[5] S. Roy,[5] G. R. Castro,[7,8] J. Rubio-Zuazo,[7,8] A. G. Ryabishchenkova,[3] K. A. Kokh,[9,10] O. E. Tereshchenko,[10,11] Z. S. Aliev,[12,13] M. B. Babanly,[14] E. V. Chulkov,[1,2,3] H. L. Meyerheim,[5] and S. S. P. Parkin[5]

[1]*Donostia International Physics Center (DIPC), 20018 San Sebastián/Donostia, Basque Country, Spain*
[2]*Departamento de Física de Materiales UPV/EHU, Centro de Física de Materiales CFM - MPC and Centro Mixto CSIC-UPV/EHU, 20080 San Sebastián/Donostia, Basque Country, Spain*
[3]*Tomsk State University, 634050 Tomsk, Russia*
[4]*Saint Petersburg State University, 198504 Saint Petersburg, Russia*
[5]*Max-Planck-Institut für Mikrostrukturphysik, Weinberg 2, D-06120 Halle, Germany*
[6]*Institut für Theoretische Physik, Johannes Kepler Universität, A 4040 Linz, Austria*
[7]*SpLine, Spanish CRG BM25 Beamline at the ESRF (The European Synchrotron), F-38000 Grenoble, France*
[8]*Instituto de Ciencia de Materiales de Madrid, Consejo Superior de Investigaciones Científicas (ICMM-CSIC), 28049 Madrid, Spain*
[9]*V. S. Sobolev Institute of Geology and Mineralogy, Siberian Branch, Russian Academy of Sciences, 630090 Novosibirsk, Russia*
[10]*Department of Physics, Novosibirsk State University, 630090 Novosibirsk, Russia*
[11]*A. V. Rzanov Institute of Semiconductor Physics, Siberian Branch, Russian Academy of Sciences, 630090 Novosibirsk, Russia*
[12]*Azerbaijan State Oil and Industry University, AZ1010 Baku, Azerbaijan*
[13]*Institute of Physics, Azerbaijan National Academy of Science, AZ1143 Baku, Azerbaijan*
[14]*Institute Catalysis and Inorganic Chemistry, Azerbaijan National Academy of Science, AZ1143 Baku, Azerbaijan*

(Received 5 January 2017; revised manuscript received 16 March 2017; published 22 May 2017)

Using surface x-ray diffraction and scanning tunneling microscopy in combination with first-principles calculations, we have studied the geometric and electronic structure of Cs-deposited Bi_2Se_3(0001) surface kept at room temperature. Two samples were investigated: a single Bi_2Se_3 crystal, whose surface was Ar sputtered and then annealed at ∼500 °C for several minutes prior to Cs deposition, and a 13-nm-thick epitaxial Bi_2Se_3 film that was not subject to sputtering and was annealed only at ∼350 °C. In the first case, a considerable fraction of Cs atoms occupy top layer Se atoms sites both on the terraces and along the upper step edges where they form one-dimensional-like structures parallel to the step. In the second case, Cs atoms occupy the fcc hollow site positions. First-principles calculations reveal that Cs atoms prefer to occupy Se positions on the Bi_2Se_3(0001) surface only if vacancies are present, which might be created during the crystal growth or during the surface preparation process. Otherwise, Cs atoms prefer to be located in fcc hollow sites in agreement with the experimental finding for the MBE-grown sample.

DOI: 10.1103/PhysRevB.95.205429

I. INTRODUCTION

In the middle of the past decade, there appeared in condensed matter physics a new branch devoted to a study of topological insulators (TIs) [1–8]. Since then it has demonstrated an explosive growth, leading to the discovery of other topological phases like Weyl [9] and Dirac [10] semimetals or the quantum anomalous Hall state [11–13]. Like the ordinary trivial insulators, TIs have an energy gap in the bulk, but unlike in those former, in TIs this gap is inverted within a certain part of the Brillouin zone as a consequence of the strong spin-orbit coupling. As a result, the TI surface hosts a gapless and linearly dispersing state, which is commonly referred to as the Dirac cone. The electrons in this state are spin-polarized and topologically protected by time reversal symmetry against backscattering on defects, which in principle could result in a nearly dissipationless spin current. Therefore TIs have an enormous potential for spintronics and quantum computation.

Topological protection at the TI surface persists under perturbations that respect time-reversal symmetry while it can be lifted by those breaking this symmetry. Both situations can be realized by adsorption of an appropriate type of foreign species at the TIs surface. Therefore, many studies have been carried out in order to understand whether and to what extent adsorption of foreign species modifies the topological surface state. The deposition of the magnetic atoms is expected to break the time-reversal symmetry and if their moments are directed perpendicularly to the surface the topological surface state must split [14]. Such a behavior is confirmed by recent *ab initio* calculations [15–17]. However its reproducible experimental confirmation is still challenging and the issue of the gap opening at the Dirac point proves to be controversial so far [18–22]. On the other hand, the deposition of nonmagnetic atoms or molecules on the TI surface does not break time-reversal symmetry but nevertheless can change a TI surface electronic [23–30] and crystal [31–33] structure significantly. As it has been evidenced by several experiments with deposition of various adsorbates on TI surfaces [23–29], the Bychkov-Rashba-split states [34], coexisting with the Dirac cone inside the energy gap, can be formed at TIs surfaces. Adsorbate-induced band bending has been proposed as a mechanism responsible for the appearance of these parabolic states, however, other studies have also related it to the expansion of the van der Waals (vdW) gap [35,36], induced by intercalation of the adsorbed species [37,38]. For certain adsorbates these states do not appear [31,32,39]. Moreover, the

adsorbate-mediated control of the Dirac point position inside the bulk band gap has been put forward [31,32], which is a new, robust and simple method as compared to those previously proposed [40–42].

In this context, it is important to note that thus far much less attention has been paid to the structural side of the problem of the adsorbate deposition at TIs surfaces. While the case of the magnetic adatoms deposition on the bismuth chalcogenides surfaces appears to be more or less understood to date [21,43–45], for the alkali metal atoms, which are often used for the doping of TI surfaces [23–29,46,47], it is hardly the case. For the deposition without subsequent annealing, the Rb adatoms on $Bi_2Se_3(0001)$ were reported to occupy hollow sites on the basis of scanning tunneling microscopy measurements [47]. However, for the thermally activated case (annealing) the results reported to date are contradictory. Authors of Ref. [23] supposed the annealing-induced partial desorption of potassium atoms from the $Bi_2Se_3(0001)$ surface, which leads to a partial recovery of the photoemission spectrum of the doped surface of the topological insulator. In stark contrast, the authors of Ref. [29] argued on partial intercalation of the chemically- and size-similar Rb atoms into the Bi_2Se_3 vdW gaps after a brief annealing, since the partial loss of the adatoms from the selected surface area revealed by scanning tunneling microscopy (STM) was accompanied by a shift of the Rb3*d* core level. Recently, the latter conclusion has been challenged by the results of *ab initio* calculations [48,49], revealing an extremely large energy penalty (several eV) for the big alkali atoms entering in the vdW gap.

In the present work, by using surface x-ray diffraction (SXRD) and STM in combination with first-principles calculations, the geometric structure and morphology of Cs adatoms deposited on the $Bi_2Se_3(0001)$ surface in submonolayer amounts is studied. The SXRD experiments indicate that in the case of the (0001) surface of Bi_2Se_3 single crystal, that was prepared by Ar^+ ion sputtering and subsequent annealing at $\sim$500 °C, at a coverage of up to about 0.4 monolayer (ML), Cs atoms occupy topmost layer Se sites, while intercalation into the vdW gap is negligible, at least without annealing the sample after deposition. Here, and in the following we refer to 1 ML as 6.74×10^{14} Cs atoms/cm^2. Simultaneously, STM images show that at the beginning of the adsorption process (and up to $\approx$0.1 ML) Cs atoms are located at the upper step edges forming one-dimensional-like structures about one nanometer in width. In accordance with first-principles simulations, occupation of the topmost Se layer sites is energetically possible if Se vacancies are present on the pristine surface, while the *fcc* hollow sites are occupied otherwise. This view is supported by the SXRD analysis of Cs deposited on a 13-nm-thick Bi_2Se_3 film grown by molecular beam epitaxy (MBE) on Si(111). It is well established that the surfaces of Bi-chalcogenides prepared by MBE are almost defect free [50]. Besides, in our experiment the MBE-grown film surface has not been treated by Ar^+ ion sputtering, while the temperature of the annealing, performed before the adsorbate deposition, has been set to $\sim$350 °C, which is much lower than the one used for the single crystal sample. In such a case, the SXRD analysis clearly shows that Cs atoms are located in *fcc*-type hollow sites (i.e., above the third layer Se atoms), which is in agreement with our *ab initio* calculations. These results suggest that the Cs adsorption site sensitively depends on the presence of surface vacancies which might be induced by the sample preparation method and/or are created during the crystal growth process.

We have also carried out first-principles calculations to elucidate the impact of the surface geometric structure and morphology on the surface electronic structure and, in particular, on the formation of Bychkov-Rashba-split electron states recently found in photoemission experiments [27,29,51].

II. SXRD AND STM EXPERIMENTS

The SXRD experiments concerned with the single crystal have been carried out at the beamline BM25b of the European Synchrotron Radiation Facility (ESRF) in Grenoble (France) [52]. After transfer into the ultrahigh vacuum chamber the Bi_2Se_3 single crystal was cleaned by mild sputtering followed by annealing at about 500 °C for several minutes as reported earlier [31]. Cs was deposited by evaporation from thoroughly outgassed and calibrated SAES dispensers while the sample was kept at room temperature. Subsequently x-ray reflections were collected under grazing incidence ($\alpha_i = 1$ deg.) of the incoming beam ($\lambda = 0.82$ Å). In total about 2300 reflections along eight crystal truncation rods (CTRs) reducing to four (1104 reflections) by symmetry equivalence (plane group $p3m1$) were collected.

Symbols in Fig. 1 represent the collected structure factor amplitudes $|F_{obs}(hk\ell)|$ along several CTRs together with the calculated ones (solid lines) based on the best fit structure model. The structure model was refined by least squares fitting of the calculated $|F_{calc}(hk\ell)|$'s to the experimental ones. Owing to the high symmetry of the structure, for each atomic layer only one z position is allowed to vary in addition to the occupancy factor (Θ) and the Debye parameter ($B = 8\pi^2\langle u\rangle^2$, where $\langle u\rangle^2$ represents the mean squared atomic displacement factor) and an overall scale factor. Figure 2(a) outlines a schematic of the structure model showing the topmost quintuple layer (QL) in side view. Small (red) and medium sized (blue) spheres represent Se and Bi atoms, respectively. The most important result is that Cs atoms replace Se atoms at the surface of the crystal, at least at the initial adsorption stage at a coverage well below 1 ML. Cs resides at a vertical distance of $d_\perp = 1.2$ Å above the plane of Se atoms corresponding to an interatomic Cs-Bi distance of 3.80 Å, which is in reasonable agreement with the Cs-Bi distance found in bulk $CsBi_2$ (4.04 Å, Ref. [53]) and with the sum of the respective atomic radii ($r_{Bi} = 1.60$ Å, $r_{Cs} = 2.60$ Å according to Slater [54]). The uncertainty of the distance determination lies in the 0.1 Å range. In addition, we find an outward expansion of the first Se-Bi interlayer spacing by $\Delta d_{12} = +12\%$, while relaxations and changes of the occupancy in deeper layers were found not to be significant. The experimental uncertainty for Δd lies in the 3 percentage points regime. The substitutional model leads to the best fit. The fit quality is measured by the unweighted residuum (R_u), which measures the average relative deviation between the observed and the calculated structure factor amplitudes [55]. Solid lines in Figs. 1(a)–1(e) represent for the best fit the calculated structure factor amplitudes ($|F_{calc}(hk\ell)|$) which follow the observed ones ($|F_{obs}(hk\ell)|$) in great detail. Figure 1(f) shows for all 1104

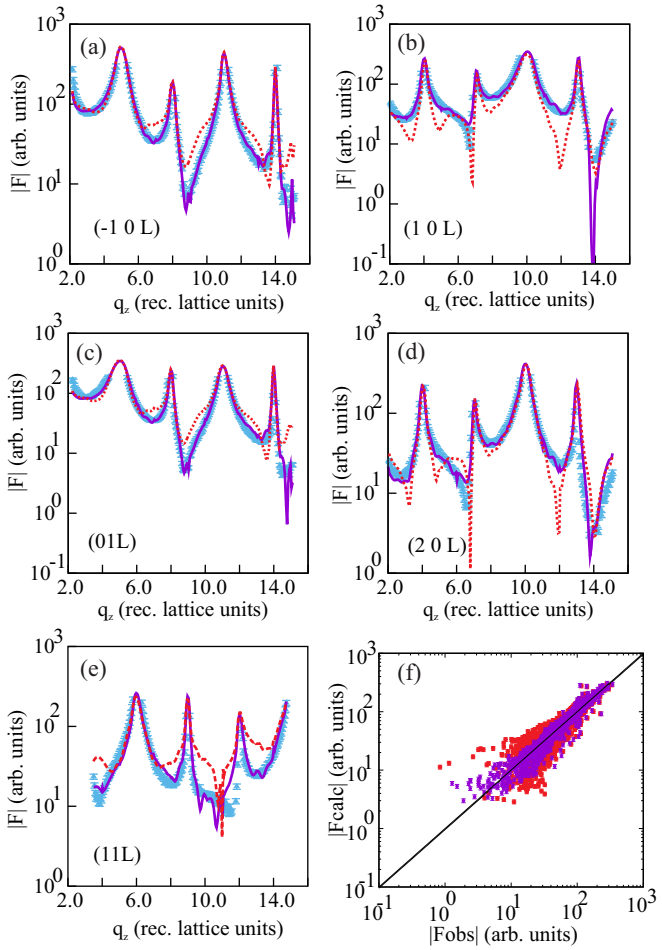

FIG. 1. (a)–(e): Experimental (symbols) and calculated (lines) structure factor amplitudes along several crystal truncation rods for about 0.4 ML of Cs atoms deposited on a single crystal $Bi_2Se_3(0001)$ surface at room temperature. The best fit represented by solid lines follows the data in all details; some disagreement is only observed at very deep minima, where the experimental resolution is not sufficient. The (red) dashed lines represent the structure factor amplitudes calculated for the model in which 0.4 ML of Cs are located in the vdW gap site. (f): Plot of $|F_{obs}|$ versus $|F_{calc}|$ for all 1104 reflections (best fit – red symbols, vdW model – dark pink symbols). The diagonal line represents the ideal condition $|F_{calc}| = |F_{obs}|$.

reflections the correlation between $|F_{obs}|$ and $|F_{calc}|$. For the substitutional model $R_u = 0.138$ is obtained. On the other hand, the fit using the structural model of the pristine sample [31,32] gives $R_u \approx 0.32$.

Models based on different adsorption sites lead to R_u values of about 0.25 for the fcc and the hcp site while we find 0.27 for the vdW gap site and 0.40 for the bridge site. These values are at least a factor of two higher than for the best fit and therefore these models can be excluded. This shows how sensitive the scattered intensity along the integer order crystal truncation rods (CTR's) is to the adsorption site. This is because of the phase contrast involved by the coherent addition of the total scattering amplitude of the substrate (F_{sub}) and the adsorbate (F_{ad}). The expression for the total scattered intensity, which is given by $I_{tot} \propto |F_{sub} + F_{ad} \times \exp[-i\phi]|^2$ contains the phase factor $\exp[-i\phi]$ related to the adsorption site. As an example, the (red) dashed lines in Figs. 1(a)–1(e) represent the $|F_{calc}(hk\ell)|$'s for the vdW site adsorption with an occupancy of 0.40. Strong deviations from the $|F_{obs}(hk\ell)|$'s are obvious, most importantly far away from the bulk Bragg reflections given by the condition $-h + k + \ell = 3n$ (n integer). Finally, in Fig. 1(f) red symbols represent the graphical correlation between $|F_{calc}(hk\ell)|$ and $|F_{obs}(hk\ell)|$, which in comparison with the best fit (dark pink symbols) exhibits a pronounced larger scatter for low magnitudes of $|F(hk\ell)|$. We have also carried out detailed calculations by varying the occupancies of the surface substitutional site (Θ_{sub}) and the vdW (Θ_{vdW}) site. The result is outlined in Fig. 3 showing the contour plot of R_u versus Θ_{sub} and Θ_{vdW}. There is a clear minimum at $\Theta_{sub} \approx 0.45$. Based on the variation of R_u an uncertainty for Θ in general is estimated to lie in the 10 percentage points regime, which is derived by considering an increase of R_u by 5 to 10% relative to the minimum as significant. Thus, in summary the analysis gives clear evidence that at this coverage Cs atoms occupy the surface substitutional site, while the occupation of different sites does not exceed 10% at most.

The SXRD experiments concerning Cs deposition on MBE grown film have been carried out using our in-house ultra-high-vacuum diffractometer operated with a Cu-K-α microfocus x-ray source and a Pilatus 2D pixel detector. The structure of the pristine film was studied earlier [32]. The sample was slightly annealed (≈350 °C) prior to Cs deposition. Note that at a temperature above approximately 420 °C rapid evaporation of the film sets in. In this case, 228 symmetrical independent reflection intensities along the (10L), (01L), (20L), and (11L) CTRs were collected under total reflection conditions of the incident beam. Data and fit are shown in Figs. 4(a)–4(e), while Fig. 4(f) schematically shows the symmetry independent part of the a*-b* plane of the reciprocal lattice. The best fit ($R_u = 0.14$) is represented by the solid lines. Note, that in this case the observed and calculated *intensities* are considered, since an *incoherent average* over two twin domains has to be taken owing to the presence of a stacking fault in the MBE grown film (see, e.g., Ref. [32]). The structure model is sketched in Fig. 2(b). Cs atoms occupy the fcc-type hollow sites, i.e., the sites above the third Se layer atoms. Here, the vertical adsorption height is equal $d_\perp = 2.1$ Å above the plane of Se atoms, corresponding to an interatomic Cs-Se distance of 3.19 Å. Comparison with the sum of the atomic radii (3.75 Å, with $r_{Se} = 1.15$ Å, $r_{Cs} = 2.60$ Å [54]) suggests that there is considerable ionicity present in the Cs-Se bond. Thus, the Cs adsorption geometry is substantially different from that found for the single crystal. In addition, we find that the expansion of the top layer spacing is larger by a factor two, namely $\Delta d_{12} = +24\%$, which we attribute that Cs now directly bonds to the top Se atoms inducing a weakening of the Se-Bi bond. As in the case of the single crystal, deeper layer distances are almost unrelaxed.

STM experiments were carried out to study the morphology of the Cs covered Bi_2Se_3 single crystal surface. Figure 5(a) shows a 400 × 400 nm^2 sized STM image ($U = -1.0$ V, $I =$ 500 pA). It reveals the (0001) surface of the Bi_2Se_3 single crystal with its characteristic 9.5 Å high steps. Bright protrusions about 1–2 nm in diameter represent Cs islands which primarily adsorb at the upper step edge of a QL, forming one-dimensional-like structures. When the upper step edges

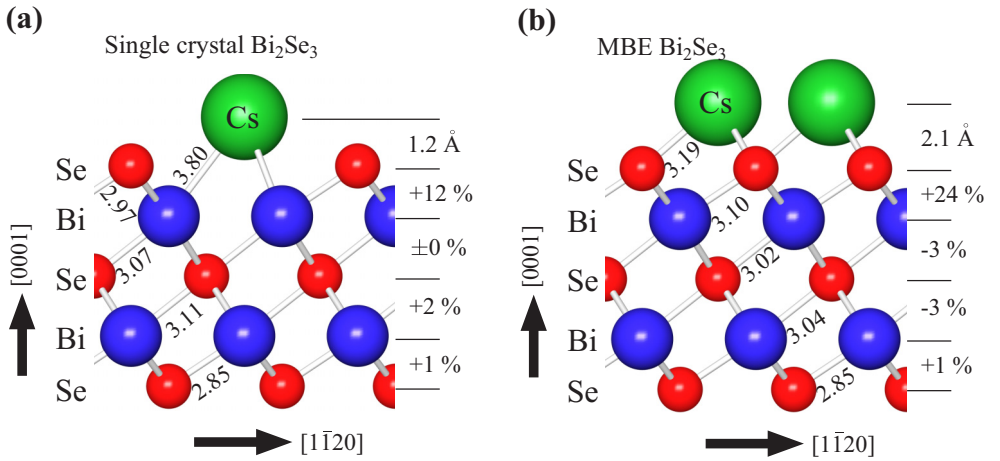

FIG. 2. Schematic of the SXRD derived Cs adsorption site geometry on single crystalline (a) and on MBE grown Bi_2Se_3 (b). Only the topmost quintuple layer is shown. Small (red) and medium sized (blue) spheres represent Se and Bi atoms, respectively. In (a) Cs occupies the topmost layer Se site and is located at a vertical height of $d_\perp = 1.2$ Å above the Se layer while in (b) Cs is located in the fcc hollow site, at 2.1 Å. Interatomic distances are given in Ångström units. Changes of the vertical interlayer spacings relative to the bulk values within the topmost QL are listed on the right.

are almost completely occupied, the subsequently deposited Cs atoms adsorb at the terraces. Figure 5(b) shows an atomically resolved STM image ($U = -1.0$ V, $I = 1$ nA) of a few islands on a terrace. Following the atomic rows near the islands suggest adsorption of Cs in the substitutional site. A line scan above such an atomic site yields an apparent height of about 0.8 Å, which is somewhat smaller than the SXRD derived value (1.2 Å), but which is only compatible with the substitutional site.

III. THEORY

To elucidate the experimental results and get deeper insight into formation of the one-dimensional-like structures along the steps we carried out *ab initio* total-energy calculations

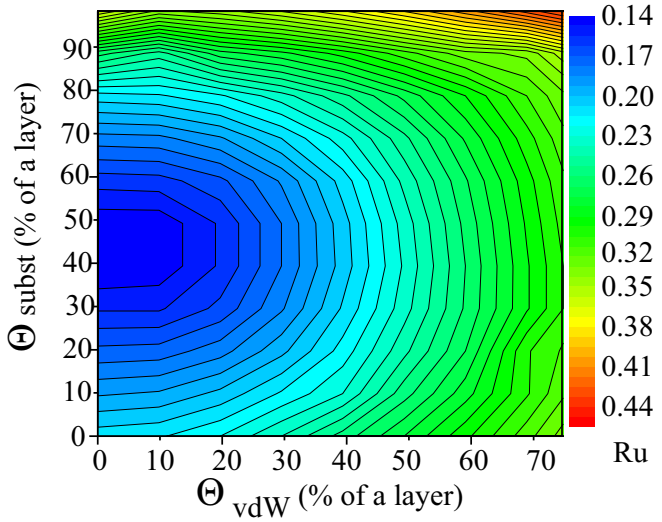

FIG. 3. Contour plot of the unweighted residuum R_u versus the occupancies of the surface substitutional site Θ_{sub} and the vdW site Θ_{vdW}. The minimum is at $\Theta_{\text{sub}} \approx 0.45$, while Θ_{vdW} approximately equals to 0.

considering various positions of Cs atoms on the stepped $Bi_2Se_3(0001)$ surface. We employed the projector augmented-wave method [56] in VASP implementation [57,58] and the generalized gradient approximation to the exchange-correlation potential [59]. The vdW interaction was taken into account within the DFT-D2 approach proposed by Grimme [60], whereas the spin-orbit interaction was neglected in all the relaxations and the structural total-energy calculations. Since the QLs of Bi_2Se_3 are only weakly bonded by vdW forces the adjacent QLs can be considered as almost independent in the sense that processes taking place on the surface QL or in between two QLs do not affect much the underlying or the nearest ones. For this reason, in the present work the study of the Cs adsorption on the surface was performed using a slab of five atomic layers (i.e., 1 QL). The isolated Cs atoms were considered using (3×3) in plane cells. To study relaxations of the adatoms near the steps, the 1-QL-thick Bi_2Se_3 stripes of at least $8a_0$ in width ($a_0 \simeq 4.13$ Å is the Bi_2Se_3 lattice constant), truncated perpendicularly to [0$\bar{1}$10] or [$\bar{1}\bar{1}$20] directions, have been considered (see Fig. 6). In the following we refer to these cases as [0$\bar{1}$10]- and [$\bar{1}\bar{1}$20]-oriented steps, respectively.

First, in the absence of any vacancy or other imperfections on $Bi_2Se_3(0001)$, the most favorable position for an isolated Cs atom is the fcc hollow, since the energies for the hcp and $bridge$ sites adsorption are by 25 and 114 meV higher, respectively. Furthermore, the top position was found to be 0.52 eV less favorable than the fcc hollow site. These results are in agreement with the SXRD structure model obtained for the surface of the Cs-deposited MBE-grown Bi_2Se_3 film. Also, they support recent STM experiments by Löptien *et al.* [47], in which chemically similar Rb atoms were deposited at room temperature on the nonannealed $Bi_2Se_3(0001)$ surface followed by rapid quenching to 4.3 K. Under these conditions Rb atoms were found to be located at only one of the two possible hollow sites. However, the calculations also show that if Se vacancies are present on the surface, they can be occupied by Cs atoms. In this case, the total energy is about 8 meV

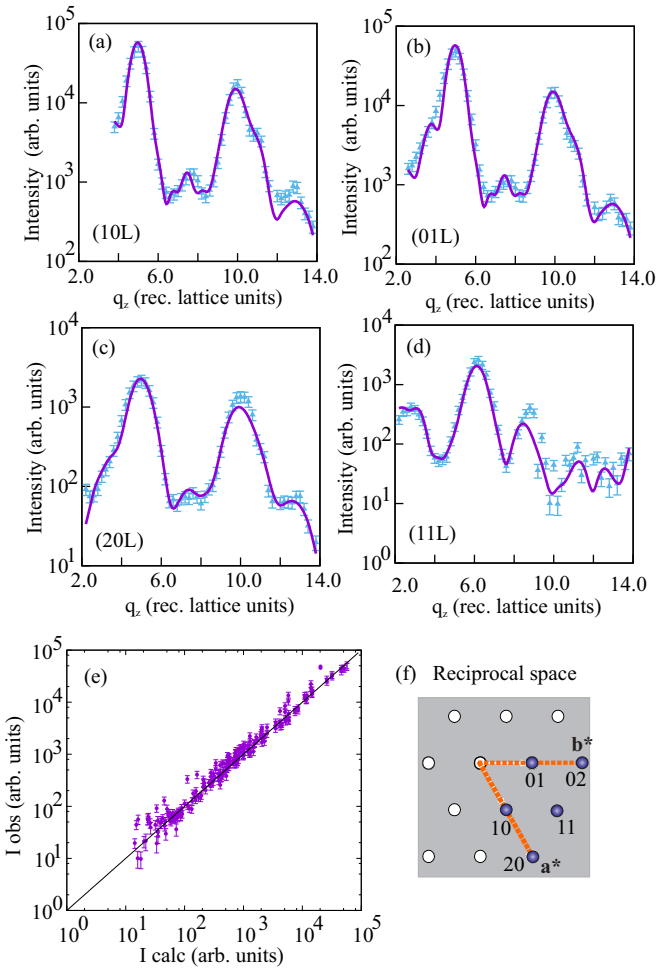

FIG. 4. (a)–(d): Experimental (symbols) and calculated (lines) intensities for about 0.8 ML of Cs atoms deposited on MBE grown $Bi_2Se_3(0001)$ at room temperature. (e): Plot of $|F_{obs}|$ versus $|F_{calc}|$ for all 228 symmetry independent reflections. The diagonal line represents the ideal condition $|F_{calc}| = |F_{obs}|$. (f): Schematic view of the $a^\star - b^\star$ plane of the $Bi_2Se_3(0001)$ reciprocal lattice emphasizing the symmetrical independent section.

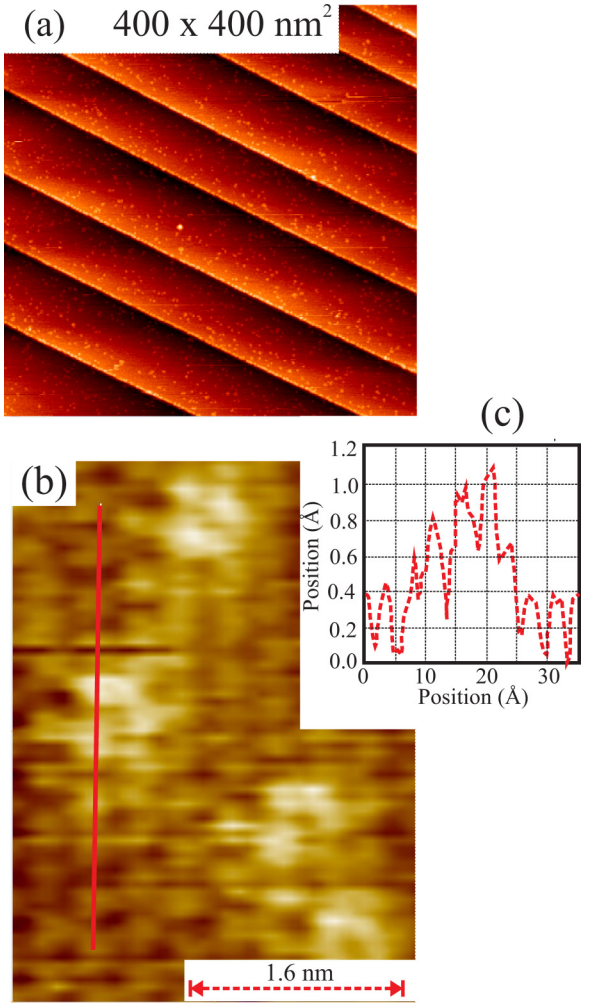

FIG. 5. (a) 400×400 nm^2 overview STM image ($U = -1.0$ V, $I = 500$ pA) of $Cs/Bi_2Se_3(0001)$. Initial adsorption of Cs leads to the formation of one-dimensional-like structures along the upper step edges of the substrate crystal. Some islands are also observed to adsorb on the terraces. (b) Atomic resolution image ($U = -1.0$ V, $I = 1$ nA) showing bright (≈ 0.8 Å) protrusions in registry with surface Se atomic sites. (c) Profile along the line in (b). Protrusions are related to Cs atoms located at Se sites with a maximum apparent elevation of approximately 0.8 Å.

lower than in the case of hollow site adsorption. This nicely supports the scenario revealed by SXRD experiments carried out on single crystal Bi_2Se_3 samples. Lattice defects such as vacancies are present as a result of the crystal growth process and by the surface preparation method employing Ar^+-ion sputtering.

Next, the formation of the one-dimensional-like structures of Cs atoms at the edge of a $Bi_2Se_3(0001)$ terrace is discussed. We model these objects by ideal Cs chains, since the simulation of the irregular agglomerations is a very complicated task. First, the chain formed by placing Cs atoms in hollow sites is considered, while the one formed by Cs atoms occupying Se vacancies is studied next. We start from the case of one Cs atom placed within the cells containing the $[0\bar{1}10]$- or $[\bar{1}\bar{1}20]$-oriented steps. It has been found that for a $[0\bar{1}10]$-step with the termination shown in Fig. 6 (see also Fig. 7 where another example of possible termination is shown) the near-edge location of Cs atom is more favorable than the one in the middle of the cell far away from the step. Namely, if a Cs atom is moved from the position marked as "2" to the near-edge located *hcp* hollow marked by "1," the total energy of the system decreases by 0.74 eV. Thus, there are step terminations for which the near-edge location of isolated Cs atoms is favorable. Therefore, Cs atoms can diffuse across the terrace, arrive at a step edge, and stay there. In the following it is illustrated that once the Cs atoms density at the terrace edge gets so high that Cs atoms cannot be considered as independent, the Coulomb repulsion comes into play which influences the Cs chain formation. It is assumed that one Cs atom is fixed near the step at the *hcp* hollow labeled as "1" in Fig. 6. As possible positions of another Cs atom, the *hcp* hollow site "2" far away from the step and two hollow positions near it, "3" (*hcp*) and "4" (*fcc*), are considered. If the second atom resides in position "4" at a distance of ~ 6.35 Å from the first one (1-4 combination), such a configuration turns out to be by 0.18 eV more favorable than the

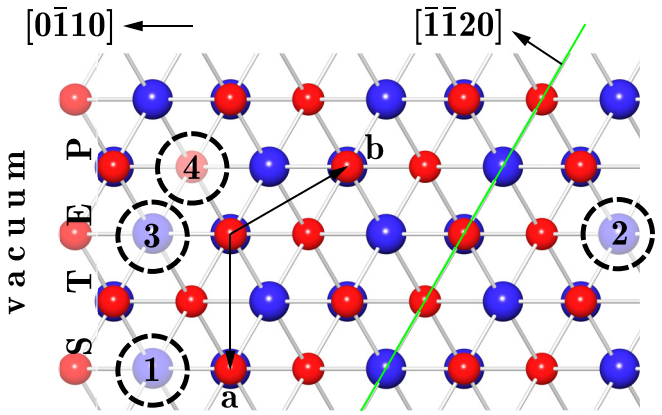

FIG. 6. Schematic view of the Bi_2Se_3(0001) surface containing [0$\bar{1}$10]-oriented step. Numbers 1–4 in circles indicate the positions of Cs atoms considered to illustrate a Cs chain formation: 1 and 3 (4)—*hcp* (*fcc*) hollows near the step, 2—*hcp* hollow far away from the step. **a** and **b** are the vectors of the planar (1 × 1) cell of the Bi_2Se_3(0001) surface. The green line shows the cut producing [$\bar{1}\bar{1}$20]-oriented step.

configuration 1-2. However, if the energy of the 1-2 or the 1-4 combination is compared with that of 1-3, where the Cs-Cs distance is equal to ∼4.13 Å, the calculations reveal that they are by ∼0.05 and 0.23 eV more favorable, respectively. This is despite the fact that in the 1-3 case both Cs atoms are located at the *hcp* hollows at the step. The increase of the total energy in the 1-3 case is attributed to the increase of the Coulomb repulsion between positively charged Cs atoms. A similar behavior is also observed for Cs atoms located at the terrace far away from the step, where they tend to stay away from each other when residing in hollow sites. Thus, the competition between the Coulomb repulsion and the energy gain at the edge is expected to govern the chain formation process: It is formed in such a way that the terrace edge accommodates a maximal amount of Cs atoms until their Coulomb repulsion energy starts to grow abruptly.

In qualitative agreement with the experimental findings, the chain formed by Cs atoms residing in Se sites can be energetically more favorable than the hollow site chain. This is demonstrated by comparing the total energies of the respective structure models using supercells constructed in such a way that they contain the same amount of atoms (the condition must be fulfilled for each atomic sort). This is illustrated in Figs. 7(a) and 7(b). It can be seen that the right-hand parts of the supercells are identical and represent one of possible terminations of the [0$\bar{1}$10]-oriented step without adsorbate. However, the left-hand sides of the cells are different. In the case of Fig. 7(a) the left step edge hosts an *fcc* hollow-site Cs chain, while in that of Fig. 7(b) the left side contains a chain of Cs atoms occupying Se sites (Cs_{Se}) in the topmost atomic layer. Note that the process of the Cs_{Se} formation, i.e., the kinetics of the vacancy formation, is not considered. In order to make the numbers of atoms in the two cases equal, two Se vacancies far away from the step are introduced in the supercell, containing the hollow-site chain. The location of the vacancies is marked by black circles and labeled by the letter "V." The dashed circle indicates a vacancy located at the opposite surface of the one-QL-thick slab. The minimum vacancy-vacancy distance in this case is equal to ∼9.36 Å. Under these conditions the energy differences between these structures solely arise from the different central regions and the regions near the steps on the left. This is because the right-hand parts of the cells are identical. It turns out that the configuration shown in Fig. 7(b) is 115 meV per Cs atom more favorable than the one in Fig. 7(a), which is in agreement with the experimentally-revealed scenario. We note that, although the one-dimensional-like structures seen

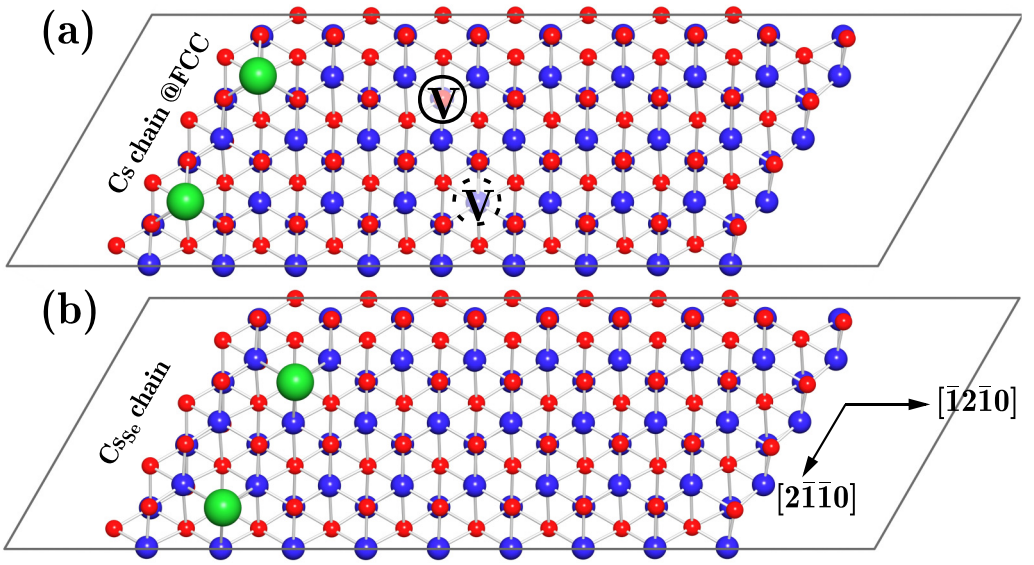

FIG. 7. Top views of the cells used for the total energy calculations containing an *fcc* hollow-site Cs chain (a) and a Cs_{Se} chain (b) near the same atomic termination of the [0$\bar{1}$10]-oriented step. The Se vacancies, introduced into the cell shown in (a), are marked by circles and letters "V," the dashed circle denoting the lateral position of the Se vacancy located at the opposite surface of the 1QL-thick slab (i.e., a Cs free surface of the slab). The right-hand side, which is defect and adatom free, exemplifies another possible atomic termination of the [0$\bar{1}$10]-oriented step.

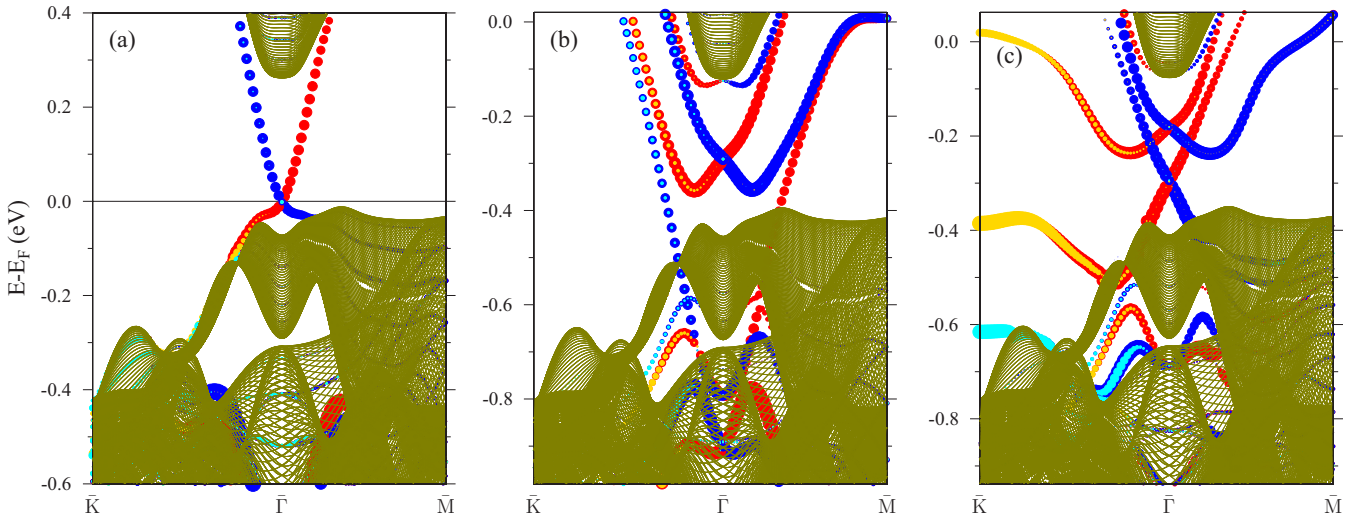

FIG. 8. Calculated spin-resolved surface band structures of the pristine Bi_2Se_3(0001) surface (a) and that with 0.25 ML of Cs located in the fcc hollow (b) or vacant Se (c) sites. The size of color circles reflects the value and sign of the spin vector Cartesian projections, with red/blue colors corresponding to the positive/negative in-plane components (that directed perpendicular to the **k** vector), and gold/cyan reflecting the out-of-plane components $+s_z/-s_z$. Green areas correspond to the bulk band structure projected onto the surface Brillouin zone.

in the STM images along the step edges do not show perfect regularity, an appearance of the more ordered structure is not excluded in the experiment since our *ab initio* total energy calculations show that the chain formation is in principle possible. For example, more regular placement of Cs atoms at the step edge could probably be achieved by appropriately adjusting experimental conditions. However, this lies beyond the scope of the present work. Thus, summarizing the results of the SXRD, STM, and DFT study discussed here, one can conclude that the hollow adsorption sites are preferred for alkali metal atoms in the case of Bi_2Se_3(0001) which is free of Se vacancies. However, if Se vacancies are present on the surface they are readily occupied by the alkali metal atoms.

On the basis of the structural model, suggesting that Cs atoms occupy the fcc hollow or topmost layer Se sites on the Bi_2Se_3(0001) surface, we have carried out electronic structure calculations taking into account spin-orbit coupling [61]. The surface was modeled by a 9-QL-thick slab and a (2×2) hexagonal supercell with four atoms per single layer which enables us to simulate an adsorbate coverage of 0.25 ML. Results of the calculations are presented in Fig. 8. Also, the electronic structure of the pristine Bi_2Se_3(0001) surface is shown for comparison. It exhibits a Dirac cone with a crossing point located at the Fermi level [see Fig. 8(a)]. Deposition of Cs atoms onto the surface results in the n doping and leads to appearance of the strongly Bychkov-Rashba-spit surface states, that were previously detected in several photoemission experiments [27,29,51]. Therewith, the Bychkov-Rashba spitting is observed for both structural models considered: (i) the fcc hollow site [Fig. 8(b)] and (ii) the substitutional Cs_{Se} position [Fig. 8(c)]. However, a better agreement with experiments is obtained for the model (i). In this case, two Bychkov-Rashba doublets are observed residing inside the Dirac cone, the $\alpha_R = 2E_R/k_R$ parameter of the lower doublet reaching a value of about 1.68 eV Å. Besides, the topological state Dirac point disappears in the bulk states due to the surface potential bending. On the other hand, within the model (ii) there is only one Bychkov-Rashba doublet clearly seen ($\alpha_R \approx 1$ eV Å). It is located at higher $k_{||}$ as compared to the topological state, whose Dirac point remains within the fundamental band gap. Comparison with previous photoemission studies [27,29,51] suggests that in these cases Cs atoms were occupying the fcc hollow sites in agreement with recent STM experiment by Löptien *et al.* [47]. Nevertheless, the surface electronic structure can be modified as in Fig. 8(c) if the Bi_2Se_3(0001) surface under Cs deposition will be prepared as it is suggested in our experiment. Thus, the structural and electronic properties of the Cs doped Bi_3Se_3(0001) surface are strongly affected by sample preparation procedure.

IV. CONCLUSIONS

We have studied the structure and morphology of submonolayer amounts of Cs on the topological insulator Bi_2Se_3. There is a dependency of the adsorption geometry on the sample growth method and the surface preparation procedure. While for a single crystal surface prepared by sputtering and annealing at high temperature an occupation of Se vacancies by Cs atoms is observed, deposition on a high-quality MBE grown film which has not been sputtered and has been annealed at much lower temperature is found to lead to the fcc hollow sites occupation. *Ab initio* calculations clearly show that the Cs atom location in the Se vacancy is energetically favorable, although the adsorption energy for the fcc hollow site is not very different. Thus, the presence of vacancies created either during single crystal growth and/or by the sample surface preparation process involving Ar^+ ion sputtering and annealing at high temperature promotes the occupancy of the Se sites by Cs atoms. In agreement with this, in the case of the MBE grown Bi_2Se_3 thin films, that are known to be almost defect free, the deposited Cs atoms adsorb in the fcc hollow sites as predicted by theory for the adsorption on ideal Bi_2Se_3(0001) surface. Such a preparation dependence of the adsorption site geometry is not uncommon. One example is the adsorption of Co on

Si(001) − (2 × 1) where a reaction to form a silicide for the sputter annealed surface or the adsorption and incorporation of Co into the undisturbed Si structure for the hydrofluoric acid etched surface has been observed [62]. Further, our total-energy calculations, performed under assumption of the vacancies presence, also confirm the experimental observation that Cs atoms can form one-dimensional-like structures along the upper step edges substituting Se atoms. Finally, on the basis of the electronic structure calculations we have shown that both interstitial and Se vacancy location of Cs atoms at the Bi_2Se_3 surface gives rise to the Bychkov-Rashba-split surface states. The strength of this splitting and the behavior of the Dirac cone strongly depend on the adsorption site and can be tuned in experiment by appropriately preparing the sample.

ACKNOWLEDGMENTS

We acknowledge financial support from DFG through priority program SPP1666 (Topological Insulators), as well as by the University of the Basque Country (Grant Nos. GIC07IT36607 and IT-756-13), the Spanish Ministry of Science and Innovation (Grant Nos. FIS2013-48286-C02-02-P, FIS2013-48286-C02-01-P, and FIS2016-75862-P) and Tomsk State University Academic D.I. Mendeleev Fund Program in 2015 (research Grant No. 8.1.05.2015). Partial support by the Saint Petersburg State University project No. 15.61.202.2015 is also acknowledged. The study has also been supported by the Russian Science Foundation (project No. 17-12-01047) in part of the single crystal growth and structural characterization. Technical support by F. Weiss is gratefully acknowledged. H.L.M., K.M., and S.R. thank the ESRF staff for the hospitality during their visit in Grenoble. We thank G. Mussler (FZ Jülich) for providing the MBE grown Bi_2Se_3 sample. Calculations were partly performed using computational resources provided by Resource Center "Computer Center of SPbU" (http://cc.spbu.ru), Donostia International Physics Center, and the SKIF-Cyberia supercomputer at the Tomsk State University.

[1] X.-L. Qi, T. L. Hughes, and S.-C. Zhang, Phys. Rev. B **78**, 195424 (2008).
[2] Y. Xia, D. Qian, D. Hsieh, L. Wray, A. Pal, H. Lin, A. Bansil, D. Grauer, Y. S. Hor, R. J. Cava, and M. Z. Hasan, Nat. Phys. **5**, 398 (2009).
[3] H. Zhang, C.-X. Liu, X.-L. Qi, X. Dai, Z. Fang, and S.-C. Zhang, Nat. Phys. **5**, 438 (2009).
[4] M. Z. Hasan and C. L. Kane, Rev. Mod. Phys. **82**, 3045 (2010).
[5] X.-L. Qi and S.-C. Zhang, Rev. Mod. Phys. **83**, 1057 (2011).
[6] S. V. Eremeev, G. Landolt, T. V. Menshchikova, B. Slomski, Y. M. Koroteev, Z. S. Aliev, M. B. Babanly, J. Henk, A. Ernst, L. Patthey *et al.*, Nat. Commun. **3**, 635 (2012).
[7] I. V. Silkin, T. V. Menshchikova, M. M. Otrokov, S. V. Eremeev, Yu. M. Koroteev, M. G. Vergniory, V. M. Kuznetsov, and E. V. Chulkov, JETP Lett. **96**, 322 (2012).
[8] P. Sessi, M. M. Otrokov, T. Bathon, M. G. Vergniory, S. S. Tsirkin, K. A. Kokh, O. E. Tereshchenko, E. V. Chulkov, and M. Bode, Phys. Rev. B **88**, 161407 (2013).
[9] A. A. Burkov and L. Balents, Phys. Rev. Lett. **107**, 127205 (2011).
[10] S. M. Young, S. Zaheer, J. C. Y. Teo, C. L. Kane, E. J. Mele, and A. M. Rappe, Phys. Rev. Lett. **108**, 140405 (2012).
[11] C.-Z. Chang, J. Zhang, X. Feng, J. Shen, Z. Zhang, M. Guo, K. Li, Y. Ou, P. Wei, L.-L. Wang *et al.*, Science **340**, 167 (2013).
[12] M. M. Otrokov, T. V. Menshchikova, I. P. Rusinov, M. G. Vergniory, V. M. Kuznetsov, and E. V. Chulkov, JETP Lett. **105**, 297 (2017).
[13] M. M. Otrokov, T. V. Menshchikova, M. G. Vergniory, I. P. Rusinov, A. Y. Vyazovskaya, Y. M. Koroteev, G. Bihlmayer, A. Ernst, P. M. Echenique, A. Arnau *et al.*, 2D Mater. **4**, 025082 (2017).
[14] Q. Liu, C.-X. Liu, C. Xu, X.-L. Qi, and S.-C. Zhang, Phys. Rev. Lett. **102**, 156603 (2009).
[15] J. Henk, M. Flieger, I. V. Maznichenko, I. Mertig, A. Ernst, S. V. Eremeev, and E. V. Chulkov, Phys. Rev. Lett. **109**, 076801 (2012).
[16] L. Chotorlishvili, A. Ernst, V. K. Dugaev, A. Komnik, M. G. Vergniory, E. V. Chulkov, and J. Berakdar, Phys. Rev. B **89**, 075103 (2014).
[17] M. M. Otrokov, E. V. Chulkov, and A. Arnau, Phys. Rev. B **92**, 165309 (2015).
[18] L. A. Wray, S.-Y. Xu, Y. Xia, D. Hsieh, A. V. Fedorov, Y. S. Hor, R. J. Cava, A. Bansil, H. Lin, and M. Z. Hasan, Nat. Phys. **7**, 32 (2011).
[19] M. R. Scholz, J. Sánchez-Barriga, D. Marchenko, A. Varykhalov, A. Volykhov, L. V. Yashina, and O. Rader, Phys. Rev. Lett. **108**, 256810 (2012).
[20] M. Ye, K. Kuroda, Y. Takeda, Y. Saitoh, K. Okamoto, S.-Y. Zhu, K. Shirai, K. Miyamoto, M. Arita, M. Nakatake *et al.*, J. Phys.: Condens. Matter **25**, 232201 (2013).
[21] T. Schlenk, M. Bianchi, M. Koleini, A. Eich, O. Pietzsch, T. O. Wehling, T. Frauenheim, A. Balatsky, J.-L. Mi, B. B. Iversen *et al.*, Phys. Rev. Lett. **110**, 126804 (2013).
[22] E. Wang, P. Tang, G. Wan, A. V. Fedorov, I. Miotkowski, Y. P. Chen, W. Duan, and S. Zhou, Nano Lett. **15**, 2031 (2015).
[23] Z.-H. Zhu, G. Levy, B. Ludbrook, C. N. Veenstra, J. A. Rosen, R. Comin, D. Wong, P. Dosanjh, A. Ubaldini, P. Syers *et al.*, Phys. Rev. Lett. **107**, 186405 (2011).
[24] H. M. Benia, C. Lin, K. Kern, and C. R. Ast, Phys. Rev. Lett. **107**, 177602 (2011).
[25] P. D. C. King, R. C. Hatch, M. Bianchi, R. Ovsyannikov, C. Lupulescu, G. Landolt, B. Slomski, J. H. Dil, D. Guan, J. L. Mi *et al.*, Phys. Rev. Lett. **107**, 096802 (2011).
[26] M. Bianchi, R. C. Hatch, J. Mi, B. B. Iversen, and P. Hofmann, Phys. Rev. Lett. **107**, 086802 (2011).
[27] T. Valla, Z.-H. Pan, D. Gardner, Y. S. Lee, and S. Chu, Phys. Rev. Lett. **108**, 117601 (2012).
[28] M. S. Bahramy, P. D. C. King, A. De La Torre, J. J. Chang, M. Shi, L. Patthey, G. Balakrishnan, P. Hofmann, R. Arita, N. Nagaosa *et al.*, Nat. Commun. **3**, 1159 (2012).
[29] M. Bianchi, R. C. Hatch, Z. Li, P. Hofmann, F. Song, J. Mi, B. B. Iversen, Z. M. Abd El-Fattah, P. Loeptien, L. Zhou *et al.*, ACS Nano **6**, 7009 (2012).
[30] A. Polyakov, C. Tusche, M. Ellguth, E. D. Crozier, K. Mohseni, M. M. Otrokov, X. Zubizarreta, M. G. Vergniory, M. Geilhufe, E. V. Chulkov *et al.*, Phys. Rev. B **95**, 180202(R) (2017).
[31] S. Roy, H. L. Meyerheim, A. Ernst, K. Mohseni, C. Tusche, M. G. Vergniory, T. V. Menshchikova, M. M. Otrokov, A. G.

Ryabishchenkova, Z. S. Aliev *et al.*, Phys. Rev. Lett. **113**, 116802 (2014).
[32] S. Roy, H. L. Meyerheim, K. Mohseni, A. Ernst, M. M. Otrokov, M. G. Vergniory, G. Mussler, J. Kampmeier, D. Grützmacher, C. Tusche *et al.*, Phys. Rev. B **90**, 155456 (2014).
[33] R. Shokri, H. L. Meyerheim, S. Roy, K. Mohseni, A. Ernst, M. M. Otrokov, E. V. Chulkov, and J. Kirschner, Phys. Rev. B **91**, 205430 (2015).
[34] Y. A. Bychkov and E. Rashba, JETP Lett. **39**, 78 (1984).
[35] M. G. Vergniory, T. V. Menshchikova, S. V. Eremeev, and E. V. Chulkov, JETP Lett. **95**, 213 (2012).
[36] S. V. Eremeev, M. G. Vergniory, T. V. Menshchikova, A. A. Shaposhnikov, and E. V. Chulkov, New J. Phys. **14**, 113030 (2012).
[37] M. Ye, S. V. Eremeev, K. Kuroda, M. Nakatake, S. Kim, Y. Yamada, E. E. Krasovskii, E. V. Chulkov, M. Arita, H. Miyahara *et al.*, arXiv:1112.5869.
[38] M. M. Otrokov, S. D. Borisova, V. Chis, M. G. Vergniory, S. V. Eremeev, V. M. Kuznetsov, and E. V. Chulkov, JETP Lett. **96**, 714 (2013).
[39] M. Caputo, M. Panighel, S. Lisi, L. Khalil, G. D. Santo, E. Papalazarou, A. Hruban, M. Konczykowski, L. Krusin-Elbaum, Z. S. Aliev *et al.*, Nano Lett. **16**, 3409 (2016).
[40] J. Zhang, C.-Z. Chang, Z. Zhang, J. Wen, X. Feng, K. Li, M. Liu, K. He, L. Wang, X. Chen, Q.-K. Xue, X. Ma, and Y. Wang, Nat. Commun. **2**, 574 (2011).
[41] T. Arakane, T. Sato, S. Souma, K. Kosaka, K. Nakayama, M. Komatsu, T. Takahashi, Z. Ren, K. Segawa, and Y. Ando, Nat. Commun. **3**, 636 (2012).
[42] T. V. Menshchikova, M. M. Otrokov, S. S. Tsirkin, D. A. Samorokov, V. V. Bebneva, A. Ernst, V. M. Kuznetsov, and E. V. Chulkov, Nano Lett. **13**, 6064 (2013).
[43] J. Honolka, A. A. Khajetoorians, V. Sessi, T. O. Wehling, S. Stepanow, J.-L. Mi, B. B. Iversen, T. Schlenk, J. Wiebe, N. B. Brookes *et al.*, Phys. Rev. Lett. **108**, 256811 (2012).
[44] D. West, Y. Y. Sun, S. B. Zhang, T. Zhang, X. Ma, P. Cheng, Y. Y. Zhang, X. Chen, J. F. Jia, and Q. K. Xue, Phys. Rev. B **85**, 081305 (2012).
[45] A. Polyakov, H. L. Meyerheim, E. D. Crozier, R. A. Gordon, K. Mohseni, S. Roy, A. Ernst, M. G. Vergniory, X. Zubizarreta, M. M. Otrokov *et al.*, Phys. Rev. B **92**, 045423 (2015).
[46] C. Seibel, H. Maaß, M. Ohtaka, S. Fiedler, C. Jünger, C.-H. Min, H. Bentmann, K. Sakamoto, and F. Reinert, Phys. Rev. B **86**, 161105 (2012).
[47] P. Löptien, L. Zhou, J. Wiebe, A. A. Khajetoorians, J. L. Mi, B. B. Iversen, P. Hofmann, and R. Wiesendanger, Phys. Rev. B **89**, 085401 (2014).
[48] A. G. Ryabishchenkova, M. M. Otrokov, V. M. Kuznetsov, and E. V. Chulkov, J. Exp. Theor. Phys. **121**, 465 (2015).
[49] M. A. Gosálvez, M. M. Otrokov, N. Ferrando, A. G. Ryabishchenkova, A. Ayuela, P. M. Echenique, and E. V. Chulkov, Phys. Rev. B **93**, 075429 (2016).
[50] S. Borisova, J. Krumrain, M. Luysberg, G. Mussler, and D. Grützmacher, Crystal Growth and Design **12**, 6098 (2012).
[51] H. M. Benia, A. Yaresko, A. P. Schnyder, J. Henk, C. T. Lin, K. Kern, and C. R. Ast, Phys. Rev. B **88**, 081103 (2013).
[52] J. Rubio-Zuazo and G. Castro, Nucl. Instrum. Methods Phys. Res., Sect. A **547**, 64 (2005).
[53] G. Gnutzmann, F. Wilhelm Dorn, and W. Klemm, Z. Anorg. Allg. Chem. **309**, 210 (1961).
[54] J. C. Slater, J. Chem. Phys. **41**, 3199 (1964).
[55] $R_u = \sum ||F_{obs}| - |F_{calc}|| / \sum |F_{obs}|$. Here, F_{obs}, F_{calc} are the experimental and calculated structure factors, respectively. The summation runs over all data points.
[56] P. E. Blöchl, Phys. Rev. B **50**, 17953 (1994).
[57] G. Kresse and J. Furthmüller, Phys. Rev. B **54**, 11169 (1996).
[58] G. Kresse and D. Joubert, Phys. Rev. B **59**, 1758 (1999).
[59] J. P. Perdew, K. Burke, and M. Ernzerhof, Phys. Rev. Lett. **77**, 3865 (1996).
[60] S. Grimme, J. Comput. Chem. **27**, 1787 (2006).
[61] D. D. Koelling and B. N. Harmon, J. Phys. C **10**, 3107 (1977).
[62] H. L. Meyerheim, U. Döbler, and A. Puschmann, Phys. Rev. B **44**, 5738 (1991).